How Much Energy Propagates Vertically in the Equatorial Oceans?

PETER R. GENT AND JAMES R. LUYTEN[1]

National Center for Atmospheric Research[2], Boulder, CO 80307

(Manuscript received 2 July 1984, in final form 2 April 1985)

ABSTRACT

Vertically propagating linear wave calculations using realistic equatorial buoyancy profiles are presented which show the percentage of the downward surface energy flux that reaches the deep equatorial oceans. The percentages vary widely depending upon the buoyancy profile and the equivalent depth but can be as low as 10% on average for equivalent depths between 1 cm and 1 m if the thermocline is sharp. This means that models with constant or weak thermocline buoyancy profiles, which allow all or most downward surface energy flux to reach the deep ocean, are very unrealistic in this respect. Another conclusion is that the observed, very low-frequency, small vertical-scale deep jets cannot be explained by linear wave theory as caused by surface forcing. It is also shown that a WKB analysis of observations can be misleading even if applied to a single vertically propagating wave in a region that excludes the main thermocline. Implications are that comparing estimates of the equivalent depth from the mixed Rossby–gravity wave dispersion relation and a WKB analysis is of little value because the error bars on both estimates are large, and that WKB estimates of downward vertical energy flux into the deep ocean can also be misleading.

1. Introduction

It has become commonplace, particularly at low latitudes, to observe low frequency energy propagating vertically in the water column, and we discuss briefly most of the observations in the next section. The propagation is manifested as a significant change in phase between velocities or temperature perturbations from instruments separated in the vertical. These phase changes imply that the observations cannot be described by a single, standing baroclinic mode (but possibly can by a sum over several modes), and consequently the low-latitude observations have mostly been analyzed as vertically propagating equatorial waves using the WKB approximation to describe the vertical structure.

In this paper we present vertically propagating linear wave calculations using a technique previously employed by Mied and Dugan (1974) and Philander (1978), namely solving the homogeneous vertical structure equation for many values of the separation constant or equivalent depth, and analyzing the results in terms of the ratio of the downward energy flux in the deep ocean to that at the ocean surface. This is done analytically for two simple buoyancy frequency profiles and numerically for three profiles representative of the different equatorial oceans in Section 3. We also study the sensitivity of our results by repeating the analysis for various other idealized profiles. This ratio or transmission coefficient is mostly small compared to one, whereas the WKB approximation assumes perfect transmission or a coefficient equal to one. Section 4 is a discussion of these calculations and their relevance for the interpretation of ocean observations. The first part of the discussion centers on estimates of the equivalent depth from the coherence phase between velocities or temperature perturbations at different depths and from the mixed Rossby–gravity wave dispersion relation with observed estimates of the frequency and zonal wavenumber. The second part is a discussion of WKB estimates of downward vertical energy flux from observations and the third part is an analysis in terms of downward and upward propagating waves that illustrates why the WKB approximation can give misleading estimates. Caveats, a summary of the calculation results and our conclusions are given in section 5.

2. Observations of vertical energy propagation in the ocean

There have been a number of reports of vertical propagation of energy in wave modes. The first of these dealt with midlatitude near-inertial oscillations. Leaman and Sanford (1975) and Leaman (1976) demonstrated that the rotation of the velocity vector with depth is associated with the vertical propagation of energy. More recently, particularly in equatorial and coastal regions, observations have been reported which show a consistent variation of the phase of a

[1] Permanent address: Woods Hole Oceanographic Institution, Woods Hole, MA 02543.

[2] The National Center for Atmospheric Research is sponsored by the National Science Foundation.

velocity component or temperature perturbation with depth. These variations have been interpreted as evidence for the vertical propagation of energy in propagating modes rather than the conventional, standing baroclinic modes. It is this interpretation that we wish to discuss.

Weisberg *et al.* (1979) and Weisberg and Horigan (1981) have analyzed moored current meter observations from the eastern equatorial Atlantic below the thermocline which show a persistent oscillation in the meridional component of velocity with a period of 31 days and zonal wavelength of 1220 km. This scale, together with the absence of a zonal component at this frequency, is consistent with a mixed Rossby–gravity wave. Observations at several depths show significant coherence with a phase which decreases with increasing depth. Using the WKB approximation, this variation in phase is interpreted as evidence for a vertically propagating wave, carrying energy downwards into the ocean, and the equivalent depth was estimated to be 2.8 cm. The equivalent depth is defined in Eq. (1).

In the equatorial Indian Ocean, Luyten and Roemmich (1982, 1985) have found, from observations in a moored array in and below the thermocline, that the zonal velocity is dominated by a very large zonal-scale oscillation with a 180-day period, while the meridional component is dominated by a 26-day oscillation. In both cases, there is a consistent vertical variation of phase which has been interpreted as vertically propagating waves. In each case, the WKB approximation is used to interpret the vertical variation in phase as a vertically propagating mode. The zonal oscillation is interpreted as a pair of equatorially trapped waves, a Kelvin wave and a first meridional-mode Rossby wave. The meridional oscillation is found to be consistent with a mixed Rossby–gravity wave, and in both cases the equivalent depth is estimated to be about 25 cm.

Lukas and Firing (1985) analyzed Hawaii–Tahiti Shuttle data from the central, upper equatorial Pacific Ocean. Analysis of temperature perturbations and dynamic heights at the annual frequency again clearly show upward phase propagation from 800 m to the thermocline. The observations are interpreted by WKB methods as a vertically propagating annual first Rossby wave, with an equivalent depth of 12.3 cm, carrying energy downwards.

There are other equatorial observations in which vertical propagation has been reported, but with somewhat less statistical significance than those discussed above. The dropped–lagged coherence technique (Hayes, 1978) has been applied to a month-long time series of repeated vertical profiles in the Indian Ocean by O'Neill (1984) and O'Neill and Luyten (1984). Evidence was found for vertical energy propagation in the meridional velocity component at two vertical wavenumber bands: upwards at 0.15 cm equivalent depth and downwards at 1.37 cm equivalent depth. Both of these components are found well beneath the thermocline in the deep water, and no source has been identified for this variability. We have introduced a convention here that we will refer to the direction in which energy propagates, which is opposite to the phase propagation direction for vertically propagating equatorial waves and coastal Kelvin waves.

Eriksen (1981, 1982) analyzed a set of vertical profiles from the western equatorial Pacific and found that the observed equatorially trapped variability is consistent with Kelvin and Rossby waves of long period and zonal wavelength, but he was unable to distinguish unambiguous vertical propagation.

In the coastal situation, Picaut (1983) analyzed monthly temperature data from the continental slope south of Abidjan and interprets the upwelling from 300 m to the surface as a vertically propagating coastal Kelvin wave. Romea and Allen (1983) have reported current meter data from the Peruvian shelf region in which the velocities showed consistent upward phase propagation. They also interpret these observations as a vertically propagating coastal Kelvin wave carrying energy downwards from the surface.

3. Calculations of vertically propagating energy flux

Philander (1978) considers the linear wave response of a hydrostatic, Boussinesq, baroclinic ocean to surface forcing. The response can be determined by separation of variables, if the forcing can be written in this manner, and Philander describes the two possible methods of proceeding. The first method is to solve for the baroclinic vertical modes first and then solve the forced horizontal structure equation using the known eigenvalues of the vertical modes. The second method is to solve, for a given frequency ω and zonal wavenumber k, the homogeneous latitudinal structure equation. This yields Hough or Hermite functions, respectively, on the sphere or equatorial β-plane. The forced vertical structure equation then has to be solved for known values of the separation constant, which are eigenvalues of the horizontal equation. The vertical structure function for vertical velocity W satisfies the forced equation (see Philander, 1978; Section D)

$$\frac{d^2W}{dz^2} + \frac{N^2(z)}{gh} W = G(z), \tag{1}$$

where N is the time and horizontal average of the buoyancy frequency, $h = h(\omega, k)$ is the known "equivalent depth" of the latitudinal mode, and $G(z)$ is the projection of the forcing onto the latitudinal mode. The physics, most of it poorly understood of how surface forcing is distributed in the vertical in the ocean surface layer by mixing, internal gravity waves, etc., is parameterized by $G(z)$. Lighthill (1969)

assumed that the forcing is confined to a mixed layer, vanishing below, whereas Wunsch (1977) assumed the forcing has an exponential decay away from the surface with a very short vertical scale. With either assumption for $G(z)$, the solution of the inhomogeneous equation (1) is confined to the forcing region, and the response below the forcing consists entirely of solutions to the homogeneous form of (1) that have to be added to the inhomogeneous part in order to satisfy the boundary condition on W at the ocean surface (often $W = 0$). The appropriate lower boundary condition is a matter of conjecture, but we follow Philander (1978) and Wunsch (1977) and impose a radiation condition of only downward propagating energy flux at the ocean floor. This is to mimic the frictional response to relatively low frequency forcing when the ray paths are so shallow that very little energy will reflect from the ocean floor (see also the discussion in Gent *et al.*, 1983, Section 6).

We have not solved a three-dimensional forced problem and have considered the simpler, but illuminating, problem of solving the homogeneous form of Eq. (1), with a given buoyancy profile $N(z)$, over a wide range of equivalent depths imposing the single boundary condition of only downward energy flux at the ocean floor. Thus

$$W = \exp[im(H)z] \quad \text{at} \quad z = H, \tag{2}$$

where H is the ocean depth and $m(z)$ is defined by

$$m(z) = N(z)/(gh)^{1/2}. \tag{3}$$

Then W is calculated by numerically integrating the homogeneous form of Eq. (1) upwards. At any z, by assuming that N is constant over the next numerical interval upwards, the solution at z can be decomposed into downward and upward propagating waves with wavenumber $m(z)$, i.e.

$$W(z) = A \exp(imz) + B \exp(-imz). \tag{4}$$

The transmission coefficient T, which is the ratio of the downward energy flux at $z = H$ to the flux of the downward energy propagating wave part of the solution at depth z, is

$$T = \frac{m(H)}{m(z)|A|^2}. \tag{5}$$

We have chosen to show the transmission coefficients between the ocean floor and surface even though, as discussed above, our solutions are valid only below the forcing region. The reason is that if the forcing is parameterized as acting in a momentum mixed layer of depth d, then we think this layer should also be thermally mixed so that N should be very small down to d. Calculations of T relative to depth d when $N(d)$ is very small and d is less than 50 m are almost identical to those we show when $N(0)$ is very small. The calculations of T are sensitive to the value of $N(0)$ and this sensitivity is illustrated using observed profiles. We show T values between the ocean floor and surface, yet these values are used to draw conclusions about the observed deep jets which occur well below the thermocline. The values of T obtained if the radiation condition is imposed well below the thermocline, or if T is calculated between well below the thermocline and the surface with the radiation condition imposed at the ocean floor, are also almost identical to those we show, so we think it valid to draw conclusions about these deep jets.

For illustrative purposes, we show T first for two simple buoyancy profiles when the integration of (1) and the values of T can be calculated analytically.

a. Piecewise constant N profile

We assume

$$N(z) = \begin{cases} N_1, & z_1 < z \\ N_2, & z_2 < z < z_1 \\ N_3, & z < z_2, \end{cases} \tag{6}$$

and corresponding values m_1, m_2 and m_3 of $m(z)$ defined by Eq. (3). The solution in the deep ocean, $W = \exp(im_3z)$, is extended upwards by matching W and dW/dz at z_2 and z_1, where dW/dz is the vertical structure function for horizontal velocity and pressure perturbation. The transmission coefficient T is the ratio of the downward energy flux for $z < z_2$ to that of the downward energy propagating part of the solution for $z > z_1$, and is given by

$$T = 4m_1m_3\{(m_1 + m_3)^2 \cos^2[m_2(z_1 - z_2)] + (m_2 + m_1m_3/m_2)^2 \sin^2[m_2(z_1 - z_2)]\}^{-1}. \tag{7}$$

If the distribution of N, Eq. (6), is taken to model the thermocline with $N_2 > \max(N_1, N_3)$, then

$$T_{\max} = 4m_1m_3(m_1 + m_3)^{-2} \quad \text{when} \quad \cos[m_2(z_1 - z_2)] = 1,$$
$$T_{\min} = 4m_1m_3(m_2 + m_1m_3/m_2)^{-2} \quad \text{when} \quad \sin[m_2(z_1 - z_2)] = 1. \tag{8}$$

This analysis differs slightly from that in Philander, because he assumed $N_1 > N_2 > N_3$. An important conclusion from (8) is that perfect transmission can occur if and only if $N_1 = N_3$, and the maxima occur when

$$gh = [(z_1 - z_2)N_2/n\pi]^2, \tag{9}$$

for integer values of n. Perfect transmission occurs when the upward and downward propagating waves in the middle layer add such that no wave is reflected from the upper interface. Also note from (8) that $T_{\min}$ is independent of h because, no matter how small h is, the vertical wavelength is large compared to the vertical scale of changes in N. Figure 1 shows

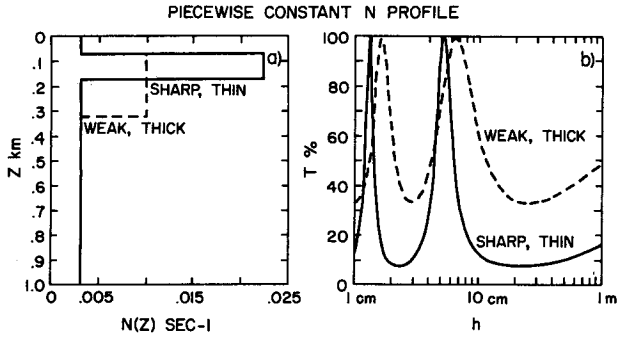

FIG. 1. (a) N profiles in upper km and (b) T as a percentage vs log$h$, 1 cm $< h <$ 1 m, for piecewise constant N profiles that represent sharp, thin (solid line) and a weak, thick (dashed line) thermocline.

the buoyancy profiles and plots of T against log$h$ for parameters that represent sharp, thin and weak, thick thermoclines. These parameters, and the first three equivalent depths of perfect transmission are given in Table 1. We emphasize again that we have chosen $N_1 = N_3$, but that if this is not true, then perfect transmission cannot occur. From Table 1 we note that the equivalent depths of maximum transmission are all less than 10 cm. No maxima occur at all for the equivalent depths of the first five vertical modes of either profile in Fig. 1a, all of which have $h > 10$ cm.

b. Sech^2N profile.

The problem can also be solved analytically if

$$m^2(z) = m_1^2 + m_2^2 \operatorname{sech}^2\sigma(z - z_T). \qquad (10)$$

This is a simplified form of the buoyancy profile used by Mied and Dugan (1974) to address the same transmission problem but for internal gravity waves (i.e., the hydrostatic assumption was not made). The simplification here means that the solutions to the homogeneous vertical structure equation (1) are Legendre functions of argument tanhσz (they are a special case of the hypergeometric functions needed in Mied and Dugan). Imposing the boundary condition of only a downward energy propagating wave far enough below z_T such that $m \approx m_1$, then the transmission coefficient far enough above z_T such that $m \approx m_1$ can be evaluated exactly as

$$T = \sinh^2(\pi m_1/\sigma)\{\cosh^2(\pi m_1/\sigma)\cos^2(\pi M/2) + \sinh^2(\pi m_1/\sigma)\sin^2(\pi M/2)\}^{-1}, \qquad (11)$$

where

$$M = (4m_2^2/\sigma^2 + 1)^{1/2}.$$

Since the buoyancy frequency takes the same value above and below the thermocline, perfect transmission is possible and it occurs when

$$\sin(\pi M/2) = 1, \quad \rightarrow gh = \frac{N_2^2}{\sigma^2 n(n+1)}, \quad \text{integer } n$$

or

$$\pi m_1/\sigma \rightarrow \infty. \qquad (12)$$

The first condition in (12) is equivalent to condition (9) for the piecewise constant profile, and gives perfect transmission for particular values of m_2/σ. The second condition in (12) occurs as either $\sigma \rightarrow 0$ so that the thermocline becomes very broad or the equivalent depth becomes very small, both of which imply that the vertical wavelength of the propagating wave is small compared to the scale of variation in the buoyancy profile. This is the condition for the WKB analysis to be valid, so that perfect transmission is to be expected. Note that this is also the reason why the minimum values of T increase as h decreases for this profile in contrast to the piecewise constant profile. Figure 2 shows the buoyancy profiles and plots of T against log$h$ for parameters that represent sharp, thin and weak, thick thermoclines. These parameters, and the first three equivalent depths of perfect transmission are also given in Table 1. These values confirm the conclusions from the piecewise constant profile that all peaks have equivalent depths less than 10 cm, and that no peaks occur for the equivalent depths of the first five vertical modes of either profile in Fig. 2a.

c. Idealized N profiles

We now illustrate the sensitivity of the transmission coefficient to both the strength and thickness of the thermocline using idealized representations of the buoyancy profile. All the profiles are piecewise linear with a ramp below the thermocline that linearly reduces the buoyancy frequency so that its value at 3 km equals its value above the thermocline. First, the thermocline thickness is kept constant at 50 m, but its strength varies with maximum N values of 1, 1.5, 2 and 2.5 $\times 10^{-2}$ s^{-1}. Figure 3 shows the various profiles and the corresponding transmission coefficients. In general, the weaker the thermocline the more downward energy flux penetrates through it,

TABLE 1. Values of the equivalent depth h that correspond to perfect energy transmission for the piecewise constant and sech^2N profiles.

	Piecewise constant			
	N_2^2 (s^{-2})	N_1^2 (s^{-2})	$z_1 - z_2$ (m)	h (cm)
Sharp, thin	5×10^{-4}	10^{-5}	100	5.16, 1.29, 0.57
Weak, thick	10^{-4}	10^{-5}	250	6.46, 1.61, 0.72
	Sech^2			
	N_2^2	N_1^2	σ(m^{-1})	h
Sharp, thin	5×10^{-4}	10^{-5}	0.02	6.33, 2.11, 1.06
Weak, thick	10^{-4}	10^{-5}	0.008	7.96, 2.65, 1.33

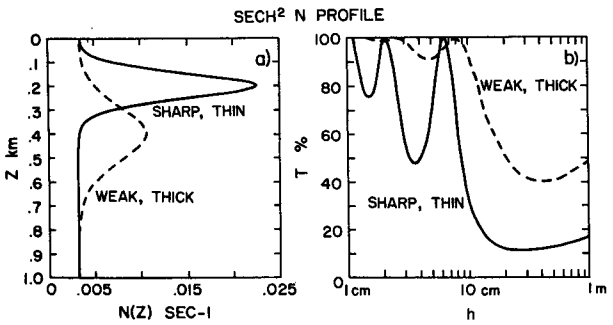

FIG. 2. As in Fig. 1 but for $\mathrm{sech}^2 N$ profile.

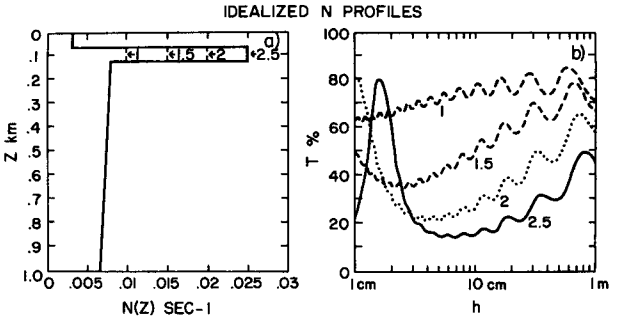

FIG. 3. (a) Idealized N profiles with thermocline peaks of 1, 1.5, 2 and 2.5 ($\times 10^{-2}$ s^{-1}), thickness 50 m and ramp down to 3 km and (b) corresponding T as a percentage vs log$h$, 1 cm $< h <$ 1 m.

although this is not true for every value of h as peaks for smaller values of h are located in different places for the different profiles. Second, we study the sensitivity of T to thermocline thickness by assuming the thermocline has a constant maximum N value of 1.5 $\times$ 10^{-2} s^{-1} and thicknesses of 50, 75 and 125 m. Figure 4 shows the various profiles and corresponding values of T. In general, the thicker the thermocline, the less downward energy flux penetrates through it, but the transmission is much less sensitive to thermocline thickness than to its strength.

d. Observed N profiles

In this section we show the transmission coefficients for observed buoyancy profiles from the three equatorial oceans. The Indian Ocean profile was calculated every 25 m by O'Neill from observations taken at 53°E between 5°N and 0.75°S during May and June 1976, and was used in the study of Gent *et al.* (1983). The upper km Pacific Ocean profile is taken from Lukas and Firing (1985) and is an average over 15 months of Hawaii–Tahiti Shuttle data at three longitudes in the central Pacific between 5°S and 5°N, and has a resolution of 10 m. The profile is extended to 4.4 km with 50 m resolution using a CTD cast near the Shuttle region. The upper 1.5 km of the Western Atlantic Ocean profile is taken from Garzoli and Katz (1981) and is a typical profile from the FGGE year. It is extended to 5 km using the Indian Ocean profile.

The Indian Ocean profile and the transmission coefficient, plotted against log of equivalent depth for h in the range 0.01 cm to 1 m, are shown in Fig. 5. The striking feature of Fig. 5b is the very small transmission coefficients for $h > 1$ cm with no values of T larger than 40% and an average value is about 10%. For $h < 1$ cm, the average value of T increases steadily to about 40% when $h = 0.1$ cm and to >75% when $h = 0.01$ cm. No peak in Fig. 5b dominates so much that, for general forcing, motion in the deep ocean should have a vertical structure corresponding to a single equivalent depth.

The transmission values shown in Fig. 5b are somewhat sensitive to the value assumed for N at the ocean surface. The value used for Fig. 5b is $N(0) = 5 \times 10^{-4}$ s^{-1}, which equals the value of N at the highest calculated point of the profile which is 12.5 m depth. If the value of $N(0)$ is reduced or increased, then the peaks in Fig. 5b remain at the same values of h, but their values decrease or increase respectively. Thus, the average transmission value of 10% is somewhat sensitive to $N(0)$, and is about 15% for 1 cm $< h <$ 1 m when $N(0)$ is multiplied by three. The appropriate value of $N(0)$ is open to debate, but we would argue that it should be less than or equal to the value just below the surface, in which case the values in Fig. 5b are upper bounds. Another possible sensitivity of the T values is the smoothness of the buoyancy profile which, for linear wave calculations, should be time and horizontally averaged. We calculated T for a smoothed profile obtained from that shown in Fig. 5a by applying an 11-point running filter below the thermocline. The values of T were essentially the same for $h > 1$ cm, and increased slightly for $h < 1$ cm. This is to be expected because the scale of variation of the buoyancy profile has increased compared to the vertical wavelength of the wave.

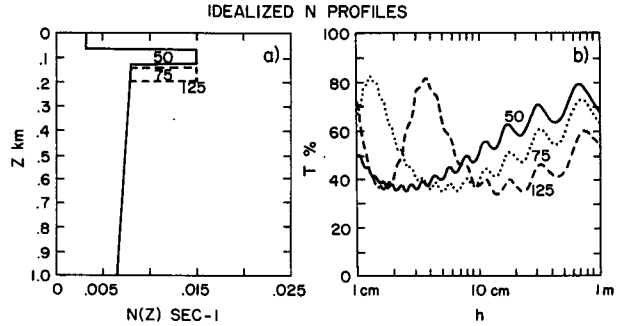

FIG. 4. As in Fig. 3 but for thermocline peak (=1.5 $\times$ 10^{-2} s^{-1}) and various thermocline thicknesses of 50, 75 and 125 m.

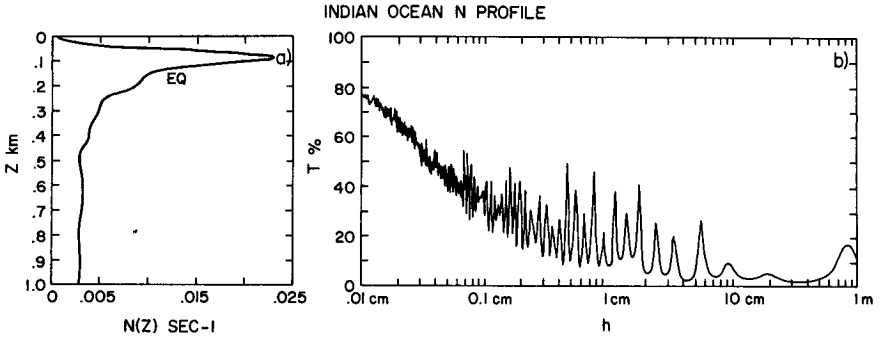

FIG. 5. (a) Observed Indian Ocean N profile in upper kilometer and (b) T as a percentage vs log$h$, 0.01 cm $< h <$ 1 m.

The Pacific Ocean profile and transmission coefficient in the range 1 cm $< h <$ 1 m are shown in Fig. 6. The values of T for this profile are considerably larger than those in Fig. 5 for the Indian Ocean profile with peaks well over 50% for h = 1–5 cm. The reason is that this profile has a large value of $N(0) \approx 5 \times 10^{-3}$ s^{-1}, has a slightly weaker, thicker thermocline and is much smoother as it is an average over many profiles. These values of T are somewhat sensitive to the value of $N(0)$ and we illustrate this in Fig. 7. It shows the values of T when the values of N between the surface and 40 m have been set equal to 5×10^{-4} s^{-1}, in order to represent a mixed layer. The values of T are smaller than those for the original profile, but the peaks in the range h = 1–5 cm remain much larger than for the less smooth Indian Ocean profile. The average value of T in this case is about 20%. The Atlantic Ocean profile and values of T in the range 1 cm $< h <$ 1 m are shown in Fig. 8. The Atlantic Ocean profile has a small value of $N(0)$, the weakest thermocline but most structure below the thermocline. In Fig. 8b there are no values of T larger than 40% and an average value is about 15%.

The lack of any peaks near one in T for $h >$ 10 cm in Figs. 5–8 conflicts with the results shown in Fig. 7 of Philander (1978) who did the same calculation using a similar equatorial buoyancy profile to ours. He predicted almost perfect transmission at h about 45 cm. We are unable to explain this conflict because we never find a value of T near one for such a large value of h when using observed buoyancy profiles. In addition we have performed three checks on the accuracy of our calculations. They are: (i) we have changed the vertical integration step size and the results are independent of this, (ii) the numerical computations reproduce the analytic results shown in Figs. 1b and 2b exactly, (iii) we calculated the equivalent depths of the vertical modes of the profiles by setting $W = 0$ at the ocean floor, integrating to the surface and plotting $W(0)$ against h. The calculations reproduced exactly the h values from independent eigenvalue solvers.

4. Discussion and interpretation of ocean observations

The values of T calculated in the last section are so much smaller than one that we now question the validity of interpreting equatorial ocean observations using the WKB technique, which assumes perfect transmission of energy. The calculations in this section analyze solutions of Eq. (1) for a single value of h. Thus they represent best observations that are well resolved in time and longitude, so that substituting the estimated values of ω and k into the dispersion

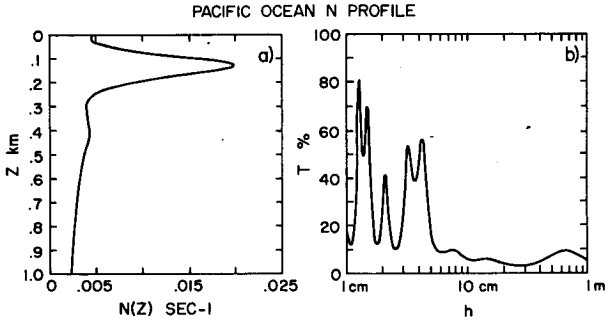

FIG. 6. As in Fig. 5 but for observed Pacific Ocean N profile, and 1 cm $< h <$ 1 m.

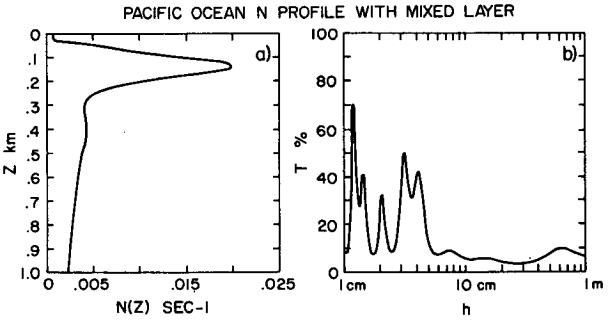

FIG. 7. As in Fig. 6 but with the N values reduced by a factor of ten in the upper 40 m.

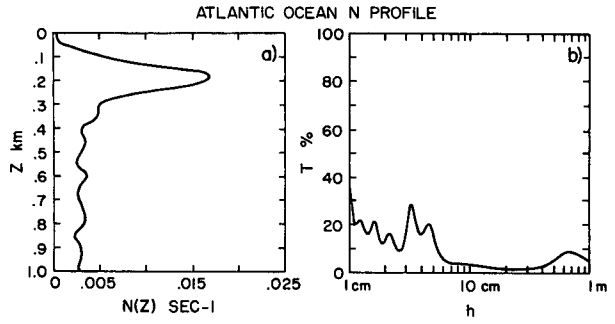

FIG. 8. As in Fig. 5 but for observed Atlantic Ocean N profile.

relation gives only one wave with a value of h between 1 cm and 1 m. A good example is Luyten and Roemmich's (1985) observations of meridional velocity, where the estimated ω and k give a mixed Rossby–gravity wave with h about 25 cm, whereas the second Rossby and gravity waves (the next gravest waves with the same symmetry) have h = 12 m and 0.08 cm, respectively. In contrast, Luyten and Roemmich's (1982) observations of zonal velocity at semi-annual frequency give the Kelvin and several Rossby waves with values of h between 1 cm and 1 m. Thus no restriction to a single vertically propagating wave can be made and Gent *et al.* (1983) have obtained vertical variations in phase that are consistent with the observations by summing Kelvin and long Rossby waves over several vertical baroclinic modes. In their model, where the forcing is complicated, a good approximation in terms of a few vertically propagating waves is not possible.

Thus, in this section we will concentrate mostly on observations of mixed Rossby–gravity waves, although the techniques discussed apply to other equatorial waves as well. The mixed Rossby–gravity waves may be generated by barotropic instability of the horizontally sheared mean currents in the thermocline. Our conclusions in this section are valid for a source in the thermocline as well as at the surface because the calculations proceed upwards from the ocean floor and so are identical below the thermocline whether they are terminated at the thermocline depth or are continued to the surface.

a. Estimates of the equivalent depth

Luyten and Roemmich (1985) calculated the coherence of the meridional velocity between 200 and 750 m, which were the shallowest and deepest instrument depths respectively. To simulate this we computed the true phase of dW/dz between 200 and 750 m, using the unsmoothed Indian Ocean buoyancy profile, in the form

$$\frac{[dW/dz(200)^*][dW/dz(750)]}{|dW/dz(200)||dW/dz(750)|} = \exp(i\phi_{\mathrm{TRUE}}), \quad (13)$$

for many values of the equivalent depth, where the asterisk means complex conjugate. The WKB estimate of the 200–750 m phase is

$$\phi_{\mathrm{WKB}} = \int_{-750}^{-200} N(z)dz/(gh)^{1/2}. \quad (14)$$

The integral in (14) is independent of h, so that $\phi_{\mathrm{WKB}} \propto h^{-1/2}$. ϕ_{TRUE} and ϕ_{WKB} are both plotted against log$h$ in Fig. 9a for h in the range 1 cm to 1 m. The two curves follow each other as a general trend, but the exact phase has much more structure than the smoothly yarying WKB estimate. The disturbing feature, however, is that ϕ_{TRUE} is multivalued in the sense that a given phase can correspond to three different values of h. Thus a measured phase need not correspond to a unique h as it must if WKB theory is used to estimate h from the observations. In fact, the WKB estimate of equivalent depth, h_{ES}, would be determined by treating the true phase, ϕ_{TRUE}, by the WKB theory, i.e.,

$$(gh_{\mathrm{ES}})^{1/2} = \int_{-750}^{-200} N(z)dz/\phi_{\mathrm{TRUE}}. \quad (15)$$

logh_{ES} is plotted against log$h$ in Fig. 9b, again for h in the range 1 cm to 1 m. For small values of h, the curves are fairly close, but as noted before, a single value of h_{ES} can correspond to three values of h. For values of h greater than 50 cm, however, the two curves diverge dramatically with h_{ES} becoming much larger than h. The reason is that ϕ_{TRUE} becomes very small for $h > 50$ cm; see Fig. 9a. The precise form of Fig. 9 depends upon the choice of 200 and 750 m, and would change if different depths were chosen. Thus, we conclude that extreme caution should be used in estimating equivalent depths using WKB theory from observed coherences, which themselves usually have large error bars. For example, Luyten and Roemmich's (1985) 95% coherence phase estimate is 62° ± 20°, which from WKB theory gives a range of h of 21–81 cm, see Fig. 9a. This conclusion applies even in the best case of only one vertically propagating wave and using WKB theory in a depth range that excludes the thermocline where the approximation

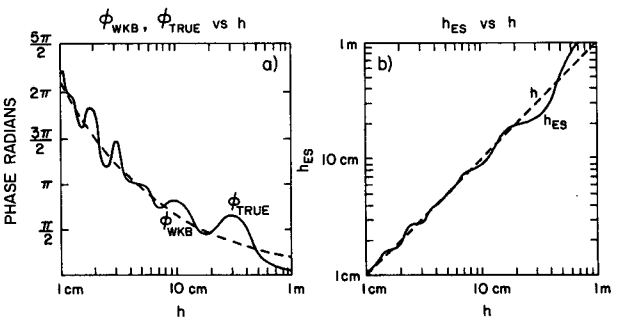

FIG. 9. (a) ϕ_{TRUE}, ϕ_{WKB} vs log$h$, 1 cm < h < 1 m, and (b) logh_{ES} vs log$h$ 1 cm < h < 1 m, for the Indian Ocean N profile.

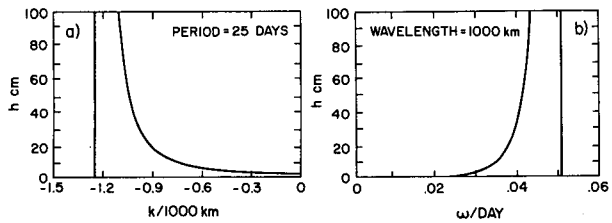

FIG. 10. Mixed Rossby–gravity wave dispersion relation, (a) h vs k for a period of 25 days, and (b) h vs ω for a wavelength of 1000 km.

obviously is not valid. An illustration of why the WKB solution does not work well for $h = 25$ cm is given in Section 4c.

Most of the mid-depth meridional velocity observations taken on the equator have been interpreted as vertically propagating mixed Rossby–gravity waves, with dispersion relation

$$(gh)^{1/2} = \omega^2/(\beta + \omega k). \tag{16}$$

Figure 10 shows plots of h against k for a period of 25 days and h against ω for a zonal wavelength of 1000 km. These period and wavelength are typical of those estimated from observations, and we note from Fig. 10 that h is very sensitive to estimates of both ω and k in this range, so that the estimates using the dispersion relation (16) must have large error bars for this particular wave. Luyten and Roemmich's (1985) 95% estimates of period and wavelength are 22–28 days and 1100–2000 km, which by (16) give the possible range of h as 2–76 cm. We conclude, therefore, that comparisons of h for the mixed Rossby–gravity waves using values estimated from the dispersion relation and WKB estimates from vertical coherence phases are of little value because both estimates have such large error bars.

Luyten and Roemmich (1985) show how to obtain better estimates of ω, k, and h using not only the observed phase differences in the vertical, but also the relative ratios in the vertical of kinetic and available potential energy. In our calculations kinetic energy $[\propto (dW/dz)^2]$ and available potential energy $[\propto N^2W^2]$ scale differently in the vertical, and neither scales like $N(z)$, and phase relationships are changed; e.g., zonal velocity and temperature perturbation are not in quadrature.

b. *Estimates of the downward vertical energy flux*

The downward vertical flux of energy is the correlation between vertical velocity and pressure perturbation, neither of which can be measured with sufficient accuracy in most oceanic situations to estimate the true flux directly. If this is so, then the flux has to be estimated using a specific model for the wave field assumed to be responsible for the observed variability. For the mixed Rossby–gravity wave the vertical flux integrated in the meridional direction is

$$\text{Wave Flux} = -\frac{\omega^4}{4\beta^{5/2}(\beta + \omega k)^{1/2}} \text{Im}[W^* dW/dz], \tag{17}$$

where the velocity W is calculated from the homogeneous form of Eq. (1). Since the function W is seldom observed directly, a local WKB approximation has often been made, as described in the previous subsection. This enables W to be related to dW/dz, and an estimate of the meridionally integrated wave energy density at a particular depth to be made. The downward vertical flux is then calculated as the product of the wave energy density and the local vertical group velocity, which is calculated from the mixed Rossby–gravity wave dispersion relation (16). The product for the mixed Rossby–gravity wave can be written in the following form, appropriate for estimation from horizontal velocity observations,

$$\text{WKB Flux} = -\frac{\omega^4}{4\beta^{3/2}(\beta + \omega k)^{1/2}} \frac{|V|^2}{N}(z), \tag{18}$$

where

$$V = \frac{\omega}{\beta^{1/2}(\beta + \omega k)^{1/2}} \frac{dW}{dz}.$$

We note that Weisberg *et al.* (1979) made a local estimate about the equator, whereas the above formula is only correct when the total energy density is used and the downward energy flux and density are integrated in the meridional direction.

The WKB flux error for a given value of h can be found by calculating the ratio of the WKB and wave fluxes from Eqs. (18) and (17). This ratio is plotted as a function of depth in Fig. 11 for the Indian Ocean N profile and $h = 25$ cm, which is the WKB estimate of Luyten and Roemmich (1985). The figure shows that the WKB flux estimate below the thermocline

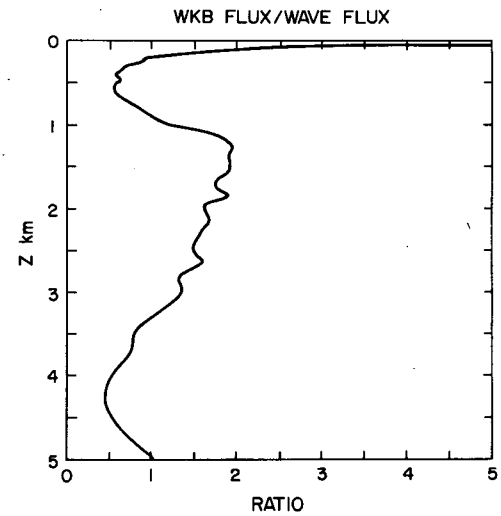

FIG. 11. Ratio of WKB to wave estimates of downward vertical energy flux vs depth 0–5 km for the Indian Ocean N profile and $h = 25$ cm.

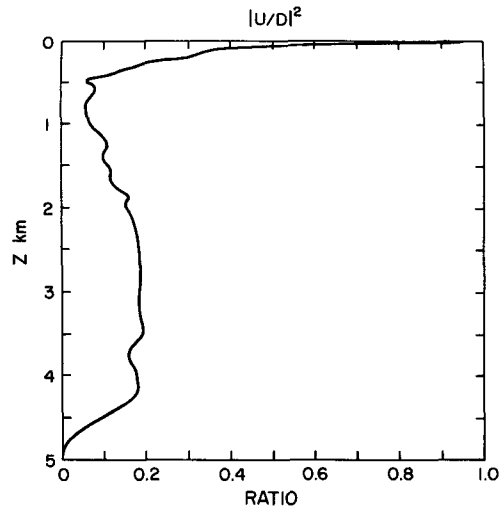

FIG. 12. $|U/D|^2$ vs depth 0–5 km for the Indian Ocean N profile and h = 25 cm.

can be too small or large by up to a factor of two depending upon the depth where it is made.

The WKB estimate can be misleading because the WKB approximation misrepresents the relationship between W and dW/dz, and it only applies when there is solely a downward energy propagating wave. For continuous buoyancy profiles, this is only true when there is perfect transmission, which is never the case for realistic profiles, as shown in Section 3d. The fact that there is not just a downward propagating wave is illustrated further in the next subsection. We also note that, for the mixed Rossby–gravity wave, both flux formulae are very sensitive to the values of ω and k, so that it is important to use the best possible estimates; see Luyten and Roemmich (1985).

c. *Analysis in terms of downward and upward propagating waves*

We now illustrate the fact that a disturbance does not consist of only a downward energy propagating wave. Consider the transformation

$$\left.\begin{aligned} W &= (D + U)/m^{1/2} \\ \frac{dW}{dz} &= im^{1/2}(D - U) \end{aligned}\right\}. \tag{19}$$

In (19) m is positive everywhere so the transformation is nonsingular, and the new variables D and U satisfy the following differential equations

$$\left.\begin{aligned} \frac{dD}{dz} - imD &= \frac{dm}{dz} U/2m \\ \frac{dU}{dz} + imU &= \frac{dm}{dz} D/2m \end{aligned}\right\}. \tag{20}$$

The WKB approximation is to ignore the right-hand sides of (20) everywhere, so that the downward and upward propagating components do not interact. The radiation condition means that U, which is the upward propagating wave when m is a constant, is zero at the ocean floor. Thus U is zero and $|D|$ is constant everywhere, and there is perfect transmission of downward energy flux. When $m^{-1}dm/dz$ cannot be neglected, however, the two components interact directly according to Eq. (20). In order to illustrate our point, we have inverted the transformation (19) at all vertical points for the solution using the Indian Ocean N profile when h = 25 cm, which from Fig. 5b, has a transmission coefficient of 3%. Figure 12 is a plot of $|U/D|^2$ against depth for this solution. It shows that U has non-negligible amplitude everywhere from 300 m to greater than 4 km, which is the range where the WKB approximation is usually applied. Above the thermocline U nearly equals D which is why the value of T is so small. We interpret this rapid change across the thermocline as indicating that most of the downward energy flux is reflected by the thermocline. This is the best justification we know of for using a one-layer model of the equatorial ocean. This type of model (e.g., Busalacchi and O'Brien 1980, 1981) imposes no downward energy flux transmission through the thermocline into the resting lower layer, so that the motion due to the surface forcing is trapped in the layer above the thermocline. This model has had success describing Kelvin waves, generated by wind changes in the west, propagating across the Pacific Ocean. We think the very large reflection of downward vertical energy flux by the equatorial thermocline is why these waves still have large amplitudes above the thermocline many thousands of kilometers away from their generation region.

5. Conclusions

We now discuss some caveats concerning the generality of our results. The first is that we have solved only the homogeneous form of the vertical structure equation and have not solved a specific three-dimensional forced problem. A three-dimensional solution is needed to describe fully how downward energy flux penetrates into the deep ocean because the ray paths are slanted and not vertical. We have considered the linear wave response to forcing using a buoyancy profile that is only a function of depth whereas the equatorial surface layer is nonlinear in the ocean and the thermocline rises and falls through the year and is certainly spatially variable. Nonlinearity is a complication we do not know how to fully overcome without resorting to a numerical model, but we think that temporal and spatial changes in the location of the thermocline will not affect the small transmission result as long as the thermocline remains sharp and thin. We have also assumed the basic state ocean to be at rest and have ignored the strong equatorial current systems. However, we think that this complication more likely reduces linear wave transmission of downward energy flux from the surface than increases it. The reason is that critical surfaces can occur in the presence of mean currents where their

velocities equal those of the vertically propagating waves and energy is absorbed at a critical surface rather than propagating through it. These currents are a source of variability themselves and instability in the equatorial undercurrent may be the source of the observed Rossby–gravity waves. If generated in the thermocline, they can propagate into the deep ocean quite freely.

Our calculations show that, for buoyancy profiles with a sharp, thin thermocline and a small value of $N(0)$, only 10–20% of the downward surface energy flux reaches the bottom of the ocean over equivalent depths between 1 cm and 1 m. The calculations are somewhat sensitive to the value assumed for $N(0)$, but insensitive to smoothing of the profiles below the thermocline. There are no peaks where the transmission is almost perfect for any value of h between 1 cm and 1 m. This last statement conflicts with the calculation of Philander (1978) who used a similar buoyancy profile and shows a peak with almost perfect transmission at $h = 45$ cm in his Fig. 7. Our first conclusion is that we find so little transmission of downward surface energy flux at the equator that any model that has perfect or high transmission is very unrealistic in this respect. This includes any model that uses a constant buoyancy profile or has a weak equatorial thermocline that does not reflect enough energy flux. Examples are McCreary (1984) for equatorial waves and Romea and Allen (1983) for coastal waves. Figure 3 shows how transmission is increased when the thermocline strength is reduced. Incidentally, another consequence of constant or weak thermocline buoyancy profiles is that the energy ray paths of vertically propagating equatorial waves descend into the deep ocean too steeply giving shorter path lengths. This means less side reflections for very low frequencies, and less time for friction to act at any frequency, and consequently a further overestimate of the downward energy flux transmission.

How much energy propagates vertically in linear models of the equatorial oceans is a rather sensitive function of four factors, only one of which has been studied in this paper. They are:

i) The spectra of ω and k in the atmospheric wind stress forcing of the ocean. Through the dispersion relations for various waves they dictate the values of the equivalent depth where the ocean is forced most strongly.

ii) How the wind stress forcing gets into the ocean. In equatorial ocean models it is often applied as a body force over a mixed layer, but atmospheric models show that vertical energy propagation into the stratosphere is sensitive to how the cumulus convection forcing in the troposphere is parameterized, see Hayashi (1976) and Chang (1976). The same will be true in the ocean and needs study.

iii) The buoyancy profile. We have shown that the transmission coefficient is a sensitive function of N especially when the thermocline is sharp and thin, and the question remains as to which is the appropriate profile to use when the thermocline has quite a large annual vertical displacement for example. The appropriate profile is that averaged over a period somewhat longer than the period of the forcing, so that the wave environment is nearly constant over a wave period. Thus, the Pacific profile is appropriate for annual forcing because it is an average over fifteen months. However, for shorter period forcing a profile with a sharper thermocline is appropriate, such as our Indian Ocean profile. Assuming that a longer averaging time gives a weaker thermocline means that, in general, more energy will propagate downwards as the period of the forcing increases.

iv) The strength of friction, especially in the thermocline. The effects of the buoyancy profile and friction act to complement each other in the following way. For short period forcing, transmission through the thermocline is small and the energy ray paths are steep, so that friction has a relatively short time to act to decrease vertically propagating energy. For long period forcing, however when the thermocline transmission is larger, the energy ray paths are shallower, so that friction has more time to act to reduce vertically propagating energy. For periods greater than about three months, energy reflections from the ocean boundaries must occur before the energy reaches the deep ocean, and less energy will propagate if these reflections are not perfect.

Rothstein *et al.* (1985) have made three-dimensional calculations to study the Kelvin wave at annual period generated by a patch of zonal wind stress. They used a body force in the upper 50 m and the Pacific buoyancy profile of Fig. 6a, and conclude that the energy transmission through the thermocline is large. We think their calculations have high energy transmission for the following reasons. They have only an annual period but a patch of wind stress that produces a spectrum of k with much power in short wavelengths or large values of k. Thus their spectrum of ω/k has much power at small values, and would be very different for forcing at a single k switched on in time, which would have much power at large values of ω/k. Studying only the Kelvin wave also produces small values of h because its dispersion relation is $\omega/k = \sqrt{gh}$, whereas for long, nondispersive Rossby waves it is $(2n + 1)\omega/k = \sqrt{gh}$. Thus their forcing spectrum and choice of wave produce small values of h which means large energy transmission. They have used the buoyancy profile with relatively large values in the mixed layer where the forcing acts. We think this is inconsistent, and our calculations in Section 3 show that this increases energy transmission considerably. We note in their calculations, however, that at annual frequency friction is efficient at reducing vertical energy propagation into the deep ocean below one km, as discussed above.

The semiannual and annual oscillations that have been observed in the equatorial oceans decay with depth and have not been observed at depths below

about 3 km, supporting our hypotheses about the combined effects of the buoyancy profile and friction. Below 3 km, however, deep jets in zonal velocity have been observed in all the equatorial oceans, and they have small vertical scale often with estimated equivalent depths of one cm or less. Also, they have not been observed propagating in the vertical, so that their frequencies must be very small, implying very shallow ray paths. We think that thermocline reflection and friction would eliminate these small vertical wavelength jets before they reached the deep ocean, so that our second conclusion is that they cannot be vertically propagating equatorial waves generated at the ocean surface. There is some possibility of their being generated in the thermocline because the energy transmission from there to the deep ocean is much higher, although barotropic instability produces perturbations with periods on the order of one or two months, not one or two years. It is then a question of how quickly they propagate vertically as to how much time friction has to act before they reach the deep ocean.

Our calculations in Section 4 apply to motions generated in the thermocline or at the surface. They show that a WKB estimate of equivalent depth can be very misleading even if the approximation is applied when only one vertically propagating wave is present and over part of the water column that excludes the main thermocline. Figure 9a shows that, when only one vertically propagating wave is present, using the WKB approximation between 200 and 750 m gives the incorrect phase. In fact, the same phase change can result from more than one h, so that the relation between them is not unique. An estimate of the equivalent depth can be misleading using the WKB estimate of phase change, as shown in Fig. 9b. Most equatorial observations of meridional velocity with periods of 25–30 days and zonal wavelengths of about 1000 km have been interpreted as mixed Rossby–gravity waves. Figure 10 shows that the calculation of h from the dispersion relation in this range is very sensitive to the precise period and zonal wavelength which are not known very accurately from observations. Our third conclusion, therefore, is that comparisons of h from the dispersion relation and a WKB phase analysis are of little value because the error bars on each estimate are so large.

Our calculations in Section 4b are of downward vertical energy flux using WKB and equatorial wave theory. Figure 11 shows that the WKB flux can be misleading because the approximation misrepresents the vertical structure and assumes that only a downward energy propagating wave is present. Our analysis in terms of D and U in Section 4c shows this is not the case; see figure 12. Our fourth conclusion, therefore, is that estimates of the downward vertical energy flux from observations using WKB theory can also be misleading.

Acknowledgment. JL would like to thank the following agencies for their support: Office of Naval Research, Ocean Sciences and Technology Division under Contract N00014-76-C-0197, and the National Science Foundation under Grants ATM 82/18595 and OCE 79/21786.

REFERENCES

Busalacchi, A. J., and J. J. O'Brien, 1980: The seasonal variability in a model of the Tropical Pacific. *J. Phys. Oceanogr.*, **10,** 1929–1951.

——, and ——, 1981: Interannual variability of the equatorial Pacific in the 1960's. *J. Geophys. Res.*, **86,** 10901–10907.

Chang, C. P., 1976: Forcing of stratospheric Kelvin waves by tropospheric heat sources. *J. Atmos. Sci.*, **33,** 740–744.

Eriksen, C. C., 1981: Deep currents and their interpretation as equatorial waves in the western Pacific Ocean. *J. Phys. Oceanogr.*, **11,** 48–70.

——, 1982: Geostrophic equatorial deep jets. *J. Mar. Res.*, **40**(Suppl.), 143–157.

Garzoli, S., and E. J. Katz, 1981: Observations of inertia-gravity waves in the Atlantic from inverted echo sounders during FGGE. *J. Phys. Oceanogr.*, **11,** 1463–1473.

Gent, P. R., K. O'Neill and M. A. Cane, 1983: A model of the semiannual oscillation in the equatorial Indian Ocean. *J. Phys. Oceanogr.*, **13,** 2148–2160.

Hayashi, Y., 1976: Nonsingular resonance of equatorial waves under the radiation condition. *J. Atmos. Sci.*, **33,** 183–201.

Hayes, S. P., 1978: Temperature fine structure observations in the Tropical North Pacific Ocean. *J. Geophys. Res.*, **83,** 5099–5104.

Leaman, K. D., 1976: Observations on the vertical polarizations and energy flux of near-inertial waves. *J. Phys. Oceanogr.*, **6,** 894–908.

——, and T. B. Sanford, 1975: Vertical energy propagation of inertial waves: A vector spectral analysis of vertical profiles. *J. Geophys. Res.*, **80,** 1975–1978.

Lighthill, M. J., 1969: Dynamic response of the Indian Ocean to onset of the southwest monsoon. *Phil. Trans. Roy. Soc. London,* **A265,** 45–92.

Lukas, R., and E. Firing, 1985: The annual Rossby wave in the central equatorial Pacific Ocean. *J. Phys. Oceanogr.*, **15,** 55–67.

Luyten, J. R., and D. H. Roemmich, 1982: Equatorial currents at semiannual period in the Indian Ocean. *J. Phys. Oceanogr.*, **12,** 406–413.

——, and ——, 1985: The 26-day oscillation in the western Indian Ocean. Submitted to *J. Phys. Oceanogr.*

McCreary, J. P., 1984: Equatorial beams. *J. Mar. Res.*, **42,** 395–430.

Mied, R. P., and J. P. Dugan, 1974: Internal gravity wave reflection by a layered density anomaly. *J. Phys. Oceanogr.*, **4,** 493–498.

O'Neill, K., 1984: Equatorial velocity profiles. Part I: Meridional component. *J. Phys. Oceanogr.*, **14,** 1829–1841.

——, and J. R. Luyten, 1984: Equatorial velocity profiles. Part II: zonal component. *J. Phys. Oceanogr.*, **14,** 1842–1852.

Philander, S. G. H., 1978: Forced oceanic waves. *Rev. Geophys. Space Phys.*, **16,** 15–46.

Picaut, J., 1983: Propagation of the seasonal upwelling in the eastern equatorial Atlantic. *J. Phys. Oceanogr.*, **13,** 18–37.

Romea, R. D., and J. S. Allen, 1983: On vertically propagating coastal Kelvin waves at low latitudes. *J. Phys. Oceanogr.*, **13,** 1241–1254.

Rothstein, L. M., D. W. Moore and J. P. McCreary, 1985: Interior reflections of a periodically forced equatorial Kelvin wave. *J. Phys. Oceanogr.* **15,** 985–996.

Weisberg, R. H., and A. M. Horigan, 1981: Low-frequency variability in the equatorial Atlantic. *J. Phys. Oceanogr.*, **11,** 913–920.

——, —— and C. Colin, 1979: Equatorially trapped Rossby–gravity wave propagation in the Gulf of Guinea. *J. Mar. Res.*, **37,** 67–86.

Wunsch, C., 1977: Response of an equatorial ocean to a periodic monsoon. *J. Phys. Oceanogr.*, **7,** 497–511.